Available online at www.sciencedirect.com
ScienceDirect
Journal of Catalysis 252 (2007) 271–280
JOURNAL OF CATALYSIS
www.elsevier.com/locate/jcat

Selective oxidation of propane and ethane on diluted Mo–V–Nb–Te mixed-oxide catalysts

B. Solsona [a,b], M.I. Vázquez [b], F. Ivars [a], A. Dejoz [b], P. Concepción [a], J.M. López Nieto [a,*]

[a] *Instituto de Tecnología Química, UPV-CSIC, Avda. Naranjos s/n, 46022 Valencia, Spain*
[b] *Departamento de Ingeniería Química, Universidad de Valencia, Dr. Moliner 50, 46100 Valencia, Spain*

Received 28 May 2007; revised 6 August 2007; accepted 23 September 2007
Available online 25 October 2007

Abstract

Te-free and Te-containing Mo–V–Nb mixed oxide catalysts were diluted with several metal oxides (SiO_2, γ-Al_2O_3, α-Al_2O_3, Nb_2O_5, or ZrO_2), characterized, and tested in the oxidation of ethane and propane. Bulk and diluted Mo–V–Nb–Te catalysts exhibited high selectivity to ethylene (up to 96%) at ethane conversions <10%, whereas the corresponding Te-free catalysts exhibited lower selectivity to ethylene. The selectivity to ethylene decreased with the ethane conversion, with this effect depending strongly on the diluter and the catalyst composition. For propane oxidation, the presence of diluter exerted a negative effect on catalytic performance (decreasing the formation of acrylic acid), and α-Al_2O_3 can be considered only a relatively efficient diluter. The higher or lower interaction between diluter and active-phase precursors, promoting or hindering an unfavorable formation of the active and selective crystalline phase [i.e., $Te_2M_{20}O_{57}$ (M = Mo, V, and Nb)], determines the catalytic performance of these materials.

Keywords: Propane oxidation; Ethane oxidation; Acrylic acid; Ethylene; Mo–V–Nb–Te diluted catalysts; Catalyst characterization (FT-Raman, XRD); α-Al_2O_3

1. Introduction

The oxidative dehydrogenation (ODH) and partial oxidation of light alkanes are drawing great interest due to the wide availability of these hydrocarbons. The ODH of ethane over redox catalysts is an interesting alternative for industrial ethylene production, because it has some advantages with respect to steam cracking or catalytic dehydrogenation [1–6]: (i) It is an exothermic reaction; (ii) it does not need a catalyst regeneration step, because catalyst regeneration occurs in situ by the oxygen feed; and (iii) relatively low reaction temperatures (350–500 °C) are required.

The partial oxidation of propane to acrylic acid also has many advantages over the current industrial process to obtain acrylic acid [6–10]. For example, propane is used instead of the more expensive propylene, and only one step is required, in contrast to the current two-step industrial process (i.e., propylene transformed into acrylic acid in two separated reactors, with acrolein as a reaction intermediate).

Although vanadium oxides supported on different materials were initially proposed as selective in the ODH of light alkanes [1–6], mixed metal oxides seem to be the most promising catalytic systems for the selective oxidative activation of C_2–C_3 alkanes [6–10]. In this way, MoVTe(Sb)NbO catalysts are the most effective catalysts in the (amm)oxidation of propane to acrylonitrile and acrylic acid [11–13] and for the ODH of ethane to ethylene [14,15] at reaction temperatures as low as 350–425 °C. These materials are characterized by the presence of an active and selective crystalline phase, that is, the orthorhombic $Te_2M_{20}O_{57}$ or $(SbO)_2M_{20}O_{56}$ (M = Mo, V, Nb), the so-called M1 phase [16–21]. In addition to this, other crystalline phases also can be observed, depending on the catalyst preparation procedure [20].

MoVTe(Sb)NbO mixed metal oxides have low surface area, which limits their potential industrial applications. The incorporation of metal oxides on a support improves the mechanical properties of the catalysts and generally modifies their catalytic behavior, which can have an unfavorable effect on catalytic per-

* Corresponding author. Fax: +34 96 3877809.
E-mail address: jmlopez@itq.upv.es (J.M. López Nieto).

0021-9517/$ – see front matter
doi:10.1016/j.jcat.2007.09.019

formance in some cases. Holmberg et al. [22] recently reported that Mo–V–Te–Nb–O catalysts diluted with silica, γ-alumina, or titania are significantly less efficient than the bulk catalyst in propane ammoxidation to acrylonitrile.

In the present paper we will describe the characterization and catalytic performance for the selective oxidative transformation of propane and ethane of Mo–V–Nb–Te mixed oxides diluted with several metal oxides. We discuss how the interaction between the diluter and the mixed metal oxide precursors during the catalyst preparation strongly influences both the nature of crystalline phases and the catalytic performance. In addition, we demonstrate that the presence of diluter has a very low influence on the selectivity to ethylene from ethane, in contrast to that observed for the selectivity to acrylic acid from propane.

2. Experimental

2.1. Catalyst preparation

Bulk Mo–V–Nb–Te mixed metal oxide catalyst was prepared by a slurry method [23]. An aqueous niobium oxalate solution was added to an aqueous solution of ammonium metavanadate, telluric acid, and ammonium heptamolybdate. The solution was rotaevaporated, dried at 100 °C overnight, and heat-treated at 600 °C in flowing N_2 for 2 h.

Diluted Mo–V–Nb–Te catalysts with a 20 wt% of the metal oxide diluter were prepared similarly as the bulk catalyst. An aqueous solution containing Mo, V, Te, and Nb salts was rotaevaporated until a wet paste was obtained, to which the support was added. After drying at 100 °C overnight, the solid was heat-treated at 600 °C in flowing N_2 for 2 h.

Commercial SiO_2 (Degussa, Aerosil-200, $S_{BET} = 186\ m^2\ g^{-1}$), α-Al_2O_3 (Pechiney, $S_{BET} = 9\ m^2\ g^{-1}$), and γ-Al_2O_3 (Sued-Chimie, $S_{BET} = 187\ m^2\ g^{-1}$) were used. ZrO_2 was prepared by hydrolysing $ZrOCl_2{\cdot}8H_2O$ with a solution of NH_4OH (at pH 7), drying at 100 °C, and calcining in air at 550 °C for 3 h ($S_{BET} = 38\ m^2\ g^{-1}$) [24]. Nb_2O_5 was obtained by calcination of Nb-oxalate in air at 550 °C for 3 h ($S_{BET} = 31\ m^2\ g^{-1}$).

Bulk and diluted Mo–V–Nb–O catalysts were also prepared similarly as the corresponding Mo–V–Nb–Te catalysts. In this case, SiO_2, α-Al_2O_3, γ-Al_2O_3 were the only metal oxide diluters studied. The denomination and characteristics of the catalysts are given in Table 1.

2.2. Catalyst characterization

Catalyst surface areas were determined by multipoint N_2 adsorption at 77 K, and data were treated in accordance with the BET method. X-ray diffraction patterns (XRD) were collected using a Philips X'Pert diffractometer equipped with a graphite monochromator, operating at 40 kV and 30 mA and using nickel-filtered CuK_α radiation ($\lambda = 0.1542$ nm).

FT-Raman spectra were recorded with an "in via" Renishaw spectrometer equipped with an Olympus microscope. The samples were excited by the 514.5 nm line of an Ar^+ laser (Spectra Physics model 171) with a laser power of 2.5 mW. The following spectrometer characteristics were used: microscope objective, 50×; spectral resolution, 2.5 cm^{-1}; integration time, 20 s per spectrum; and 50 scans. All samples were measured without previous activation. Raman spectra were obtained at different points in each sample to determine homogeneity and/or heterogeneity of the sample. The spatial resolution of each analysis was about 0.4 μm.

2.3. Catalytic tests

The catalytic experiments were carried out at atmospheric pressure, in the 340–420 °C range, using a fixed-bed quartz tubular reactor (20 mm i.d., 400 mm long). Catalyst samples were introduced in the reactor diluted with silicon carbide to maintain a constant volume in the catalytic bed. The feed consisted of a mixture of $C_3H_8/O_2/He/H_2O$ (with a molar ratio of 4/8/58/30), $C_3H_6/O_2/He/H_2O$ (with a molar ratio of 1.7/6.8/76.5/15), or $C_2H_6/O_2/He$ (with a molar ratio of 30/10/60 to 30/30/40). The amount of catalyst was varied from 0.2 to 2 g to obtain several contact times. Reactant and products were analysed by gas chromatography using two packed columns: molecular sieve 5 Å (2.5 m) and Porapak Q (3 m). Blank runs showed no conversion in the temperature range studied [15,20].

3. Results and discussion

3.1. Catalyst characterization

The characteristics of bulk and diluted catalysts are summarized in Table 1. The XRD patterns of the Te-containing and Te-free Mo–V–Nb catalysts are shown in Fig. 1. In all cases, the catalysts show the presence of a peak at $2\theta = 21.8$–$22.0°$ characteristic of oxidic bronzes with an interplanar distance of ca. 4 Å.

The XRD patterns of Te-containing catalysts suggest the presence of the orthorhombic $Te_2M_{20}O_{57}$ (M1 phase) and the pseudo-orthorhombic $Te_{0.33}MO_{3.33}$ (M2 phase) as the main crystalline phases (Fig. 1, patterns a–f), even though they present different relative intensities for their corresponding most important reflections. A first estimation on the variation of the amount of each phase in these catalysts was obtained based on the variation in intensity of the reflections observed at $2\theta = 27.2°$ and 22.0° ($I_{27.2}/I_{22.0}$, related to the presence of the M1 phase) or the reflections observed at $2\theta = 28.2°$ and 22.0° ($I_{28.2}/I_{22.0}$, related to the presence of the M2 phase). The resulting values are summarized in Table 1. Accordingly, the presence of the M1 phase decreases with the incorporation of diluter, especially in the case of ZrO_2- or Nb_2O_5-containing samples. On the other hand, the formation of M2 phase seems to be favored in SiO_2-, ZrO_2-, or Nb_2O_5-containing samples with respect to the undiluted catalyst.

Note that besides the M1 and M2 phases and the corresponding crystalline metal oxide diluter (α-Al_2O_3 and traces of Nb_2O_5 or ZrO_2), other crystalline phases were detected as well. $Al_2(MoO_4)_3$ (JCPDS: 23-764) is clearly observed in the γ-Al_2O_3-containing catalyst (Fig. 1A, pattern c), and $(V_{0.07}Mo_{0.93})_5O_{14}$ (JCPDS: 31-1437), $Nb_{0.09}Mo_{0.91}O_{2.8}$

Table 1
Characteristics of bulk and diluted (20 wt% of support) MoVTeNbO catalysts

Catalyst	Diluter	Surface area (m^2/g)	Mo/V/Nb/Te atomic ratio[a]	Crystalline phases (XRD)[b]	$I_{27.2}/I_{22.0}$ ratio (XRD)[c]	$I_{28.2}/I_{22.0}$ ratio (XRD)[d]
CT-1	–	5	1/0.22/0.13/0.23	$Te_2M_{20}O_{57}$, $Te_{0.33}MO_{3.33}$	0.29	0.66
CT-2Si	SiO_2	21	1/0.21/0.13/0.22	$Te_{0.33}MO_{3.33} > Te_2M_{20}O_{57}$	0.17	0.94
CT-3Al	γ-Al_2O_3	24	1/0.26/0.13/0.25	$Te_2M_{20}O_{57} > Te_{0.33}MO_{3.33}$, $Al_2(MoO_4)_3$	0.20	0.44
CT-4aAl	α-Al_2O_3	6	1/0.24/0.13/0.24	$Te_2M_{20}O_{57}$, $Te_{0.33}MO_{3.33}$, α-Al_2O_3	0.24	0.57
CT-5Nb	Nb_2O_5	9	1/0.23/0.22/0.23	$Te_{0.33}MO_{3.33} > Te_2M_{20}O_{57}$, $> M_5O_{14}$, $TeMo_5O_{16}$	0.08	0.96
CT-6Zr	ZrO_2	7	nd	$Te_{0.33}MO_{3.33} > Te_2M_{20}O_{57}$, M_5O_{14}, $TeMo_5O_{16}$	0.10	0.88
C-7	–	6	1/0.22/0.13/0	M_5O_{14}, $Mo_{0.67}V_{0.33}O_2$	–	–
C-8Si	SiO_2	31	1/0.22/0.13/0	M_5O_{14}, $Mo_{0.67}V_{0.33}O_2$	–	–
C-9Al	γ-Al_2O_3	35	1/0.22/0.13/0	M_5O_{14}, $Mo_{0.67}V_{0.33}O_2$, $Al_2(MoO_4)_3$		
C-10aAl	α-Al_2O_3	6	1/0.22/0.13/0	M_5O_{14}, $Mo_{0.67}V_{0.33}O_2$, α-Al_2O_3	–	–

[a] Atomic ratio obtained by atomic absorption.
[b] $Te_2M_{20}O_{57}$, $Te_{0.33}MO_{3.33}$ and M_5O_{14} with M = Mo, V and/or Nb.
[c] Estimation of the relative amount of $Te_2M_{20}O_{57}$ (M1 phase).
[d] Estimation of the relative amount of $Te_{0.33}MO_{3.33}$ (M2 phase).

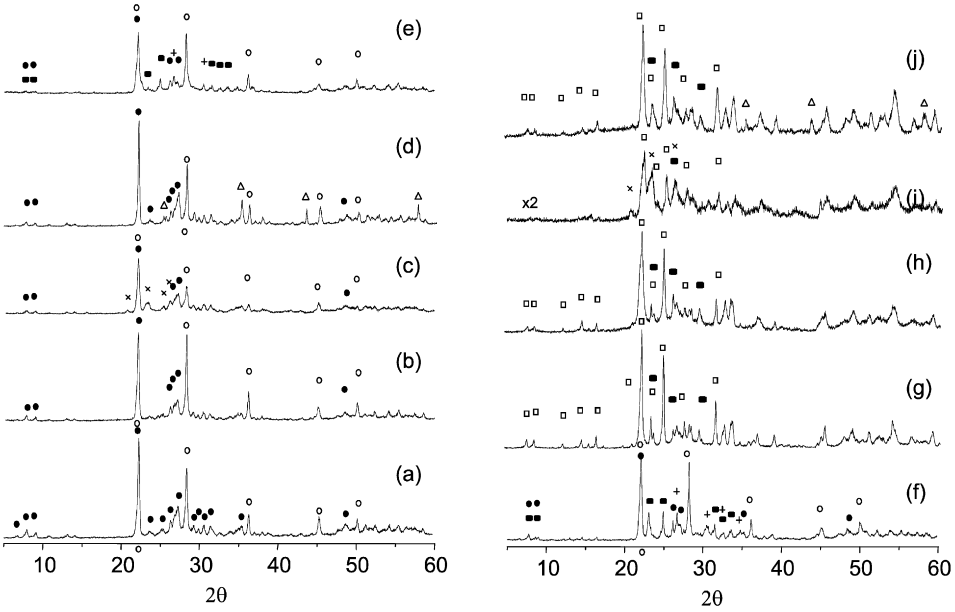

Fig. 1. XRD patterns of bulk and diluted MoVNb(Te)O catalysts: (a) CT-1; (b) CT-2Si; (c) CT-3Al; (d) CT-4aAl; (e) CT-5Nb; (f) CT-6Zr; (g) C-7; (h) C-8Si; (i) C-9Al; (j) C-10aAl. Symbols: $Te_2M_{20}O_{57}$ (M1 phase) (●); $Te_{0.33}MO_{3.33}$ (M2 phase) (○); $TeMo_5O_{16}$ (+); $(V_{0.07}Mo_{0.93})_5O_{14}$ and/or $Nb_{0.09}Mo_{0.91}O_{2.8}$ (■); α-Al_2O_3 (△); $Al_2(MoO_4)_3$ (×); $Mo_{0.67}V_{0.33}O_2$ (□).

(JCPDS: 27-0310), and $TeMo_5O_{16}$ (JCPDS: 31-874) can be seen in Nb_2O_5- or ZrO_2-diluted MoVNbTeO catalysts (Fig. 1, patterns e and f, respectively).

The XRD patterns of bulk and diluted Mo–V–Nb mixed-oxide catalysts are also shown in Fig. 1 (patterns g–j). These patterns suggest the presence of $(Mo_{0.93}V_{0.07})_5O_{14}$ (JCPDS: 31-1437) and/or $Nb_{0.09}Mo_{0.91}O_{2.8}$ (JCPDS: 27-0310) in addition to $Mo_{0.67}V_{0.33}O_2$ (JCPDS: 30-0849), although with a different relative intensity for the most important reflections. Furthermore, the XRD pattern of γ-Al_2O_3-diluted MoVNbO catalyst (C-9Al) also suggests the presence of $Al_2(MoO_4)_3$ (JCPDS: 23-764), whereas the characteristic diffraction peaks of α-Al_2O_3 (JCPDS: 10-0173) remains in the α-Al_2O_3-diluted sample (Fig. 1, pattern j).

The Raman spectrum of bulk Mo–V–Nb–Te catalyst, shown in Fig. 2 (spectrum a), exhibits an intense Raman band at 874 cm^{-1} with a broad shoulder toward lower frequencies, in the 770–840 cm^{-1} Raman region, and a weak shoulder toward higher frequencies, at around 970 cm^{-1}. In addition to these, bands at lower frequencies (470 and 437 cm^{-1}) are also observed. This spectrum is similar to those reported previously [13,25]. The shoulder at 970 cm^{-1} can be assigned to stretching vibrations of terminal Mo=O and V=O bonds [26], whereas the bands at 770–880 cm^{-1} appear in a typical regime of asymmetric Me–O–Me bridge stretching modes, and the low-frequency bands (around 470 cm^{-1}) appear in a typical regime of their symmetric Me–O–Me bridge stretching modes.

For comparative purposes, the Raman spectra of two bulk MoVTeNbO samples containing pure M1 or pure M2 phase also have been included (Fig. 2, spectra b and c), because, as reported for the XRD pattern of bulk Mo–V–Nb–Te sample, it shows the presence of $Te_2M_{20}O_{57}$ (M1 phase) and

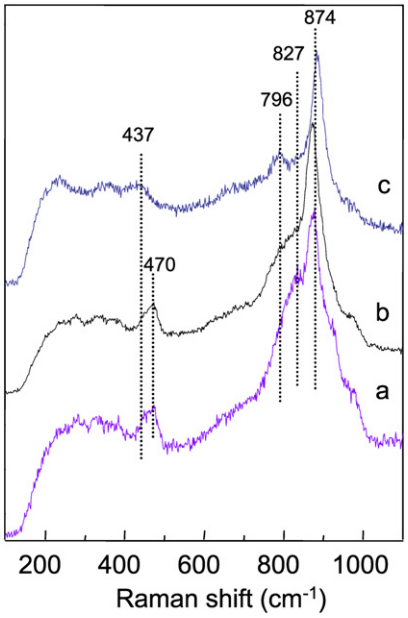

Fig. 2. FT-Raman spectra of Mo–V–Nb–Te catalysts: (a) CT-1; (b) pure M1 phase; (c) pure M2 phase.

$Te_{0.33}MO_{3.33}$ (M2 phase). The most intense Raman band at 874 cm^{-1} is present on both pure phases, whereas different Me–O–Me stretching modes can be observed in both crystalline phases. In this way, bands at 796 and 437 cm^{-1} are observed in the M2 phase and are shifted to higher frequencies (827 and 470 cm^{-1}) in the M1 phase.

Raman spectra of diluted Mo–V–Nb–Te samples are shown in Fig. 3. Both the SiO_2- and α-Al_2O_3-containing catalysts appear to be quite homogeneous, with Raman spectra similar to those seen for the undiluted catalyst (Fig. 3, spectra a and b, respectively), although a higher contribution of the bands at 796 and 437 cm^{-1} can be seen in the SiO_2-containing sample. Accordingly, a greater contribution of the M2 phase can be inferred in these catalysts, as previously suggested by XRD measurements (see Table 1).

On the other hand, some heterogeneity with the presence of other oxide phases can be seen in catalysts diluted with γ-Al_2O_3, Nb_2O_5, or ZrO_2 (Fig. 3, spectra c–h). Two types of Raman spectra are observed in these cases. For the γ-Al_2O_3-containing catalyst, characteristic bands related to M1 and M2 (Fig. 3, spectrum c) are seen; however, a different Raman spectrum characterized by the presence of bands at 974, 818, and 370 cm^{-1} also can be obtained in some particles (Fig. 3, spectrum d). According to the literature, the broad band centered at 950 cm^{-1} has been attributed to a molybdenum–support interaction in γ-Al_2O_3-supported molybdenum oxides [27], whereas Raman bands at 1006 and 380 cm^{-1} have been assigned to the formation of $Al_2(MoO_4)_3$ [28]. In our case, the band at 1006 is overlapped by the strong Raman band centered at 970 cm^{-1}.

The Raman spectra of Nb_2O_5-containing Mo–V–Nb–Te catalyst (Fig. 3, spectra e and f) show the presence of the M2 phase (Raman bands at 796 and 437 cm^{-1}). Moreover, these spectra suggest some heterogeneity. In this way, the presence of a broad, intense Raman band at 690 cm^{-1} indicates particles containing Nb_2O_5 oxide (Fig. 3, spectrum f) [29].

For the ZrO_2-containing sample, two types of spectra can be observed (Fig. 3, spectra g and h). The first type suggests the presence of the M2 phase (with the Raman bands at 796 and

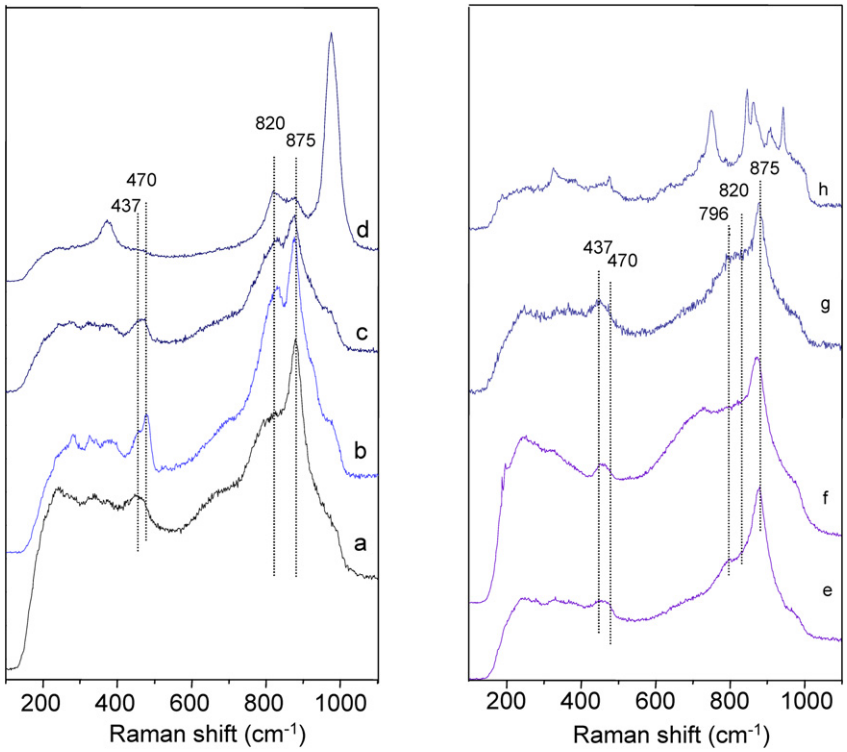

Fig. 3. FT-Raman spectra of diluted MoVTeNbO samples: CT-2Si (a); CT-4aAl (b); CT-3Al (c and d); CT-5Nb (e and f); CT-6Zr (g and h).

437 cm^{-1}) (Fig. 3, spectrum g); the second indicates the presence of $ZrMo_2O_8$ (characterized by strong Raman bands at 748, 944, and 1000 cm^{-1} [30]), together with bands at 909, 863, 845, 760, 715, and 685 cm^{-1} (Fig. 3, spectrum h). The band at 637–640 cm^{-1} is related to ZrO_2 [30], whereas (as discussed later) the rest of these bands correspond to Mo–V–Nb mixed oxide, similar to those observed on Te-free catalysts. Based on the XRD results, it has been proposed that the formation of the M2 crystalline phase is mainly favored over the M1 phase in the presence of Nb_2O_5 or ZrO_2. The Raman spectra of these catalysts show partial incorporation of molybdenum species to the metal oxides used as diluters.

The Raman spectra of bulk and diluted Mo–V–Nb catalyst are shown in Fig. 4. Bands at 980, 909, 863, 845, 715, 685, 463,

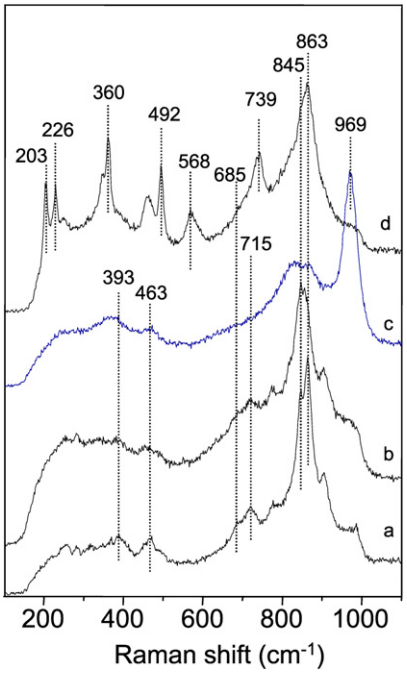

Fig. 4. FT-Raman spectra of bulk and diluted Mo–V–Nb catalysts: C-7 (a); C-8Si (b); C-9Al (c); C-10aAl (d).

and 393 cm^{-1} can be seen in all samples. These bands can be related to a Mo–V–Nb mixed oxide [31–33], as suggested from the corresponding XRD patterns. Bands at 970, 900, 850, and 710 cm^{-1} have been attributed to Mo_5O_{14}; some of these shift to 970, 920, 855, 817, and 610 cm^{-1} for $(Mo_{0.8}V_{0.1}W_{0.1})_5O_{14}$ [32,33]. Accordingly, M_5O_{14} (M = Mo, V, and/or Nb) are mainly formed in our Mo–V–Nb catalysts, with the shift of the bands observed in our case explained by the different concentrations of transition metal ions [32].

In addition to these, new bands at 969, 818, and 365 cm^{-1} can be seen in the γ-Al_2O_3-diluted Mo–V–Nb–O catalyst (Fig. 4, spectrum c), whereas bands at 739, 568, 492, 459, 360, 344, 226, and 203 cm^{-1} are observed on the sample diluted with α-Al_2O_3 (Fig. 4, spectrum d). The former bands are associated with the presence of $Al_2(MoO_4)_3$ [28]; the latter, with the presence of polymolybdates [27]. However, and in addition to this, other Mo–V–Nb mixed oxides [i.e., $(Mo_{0.93}V_{0.07})_5O_{14}$, $Nb_{0.09}Mo_{0.91}O_{2.8}$ or $Mo_{0.67}V_{0.33}O_2$] also can be formed, in agreement with the XRD results. Accordingly, M_5O_{14}-type crystals (M = Mo, V, and Nb), rather than M1-/M2-type crystalline phase, can be inferred in the absence of tellurium cations.

3.2. Catalytic results

3.2.1. Propane and propylene oxidation

Blank tests in the propane oxidation using the supports alone (α-Al_2O_3, γ-Al_2O_3, Nb_2O_5, ZrO_2, SiO_2) were carried out at 400 °C and with a contact time of 600 $g_{cat}\,h\,mol_{C_3}^{-1}$. In all cases, the propane conversion achieved did not reach 1.0%.

Table 2 summarizes the catalytic results obtained in the oxidation of propane over bulk and diluted catalysts at 400 °C. Significant differences can be seen among the catalysts tested. Acrylic acid, propylene, acetic acid, carbon monoxide, and carbon dioxide were the main reaction products on Te-containing catalysts, with acetone and acrolein as minor products (the carbon balance of all catalytic tests was 100 ± 3%). However, the presence of a diluter had a negative influence on the selectivity to acrylic acid on these catalysts. Also note that both the cat-

Table 2
Oxidation of propane on bulk and diluted Mo–V–Nb–(Te) mixed oxide catalysts[a]

Catalyst	W/F[b]	Propane conversion (%)	Selectivity (%)					STY_{AA}[c]	STY'_{AA}[d]
			Acrylic acid	Propylene	Acetic acid	CO	CO_2		
CT-1	300	37.0	68.0	6.8	3.1	8.8	13.2	59	59
CT-2Si	600	19.3	38.3	11.9	3.7	16.1	29.7	8.7	11
CT-3Al	600	31.2	23.6	6.4	4.4	20.2	45.0	8.7	11
CT-4aAl	600	30.2	57.2	7.2	3.8	10.9	20.5	21	27
CT-5Nb	600	24.1	22.5	8.6	3.5	23.6	41.6	6.3	7.9
CT-6Zr	600	11.6	8.7	16.0	1.1	26.7	47.2	1.2	1.5
C-7	300	15.0	0	12.7	3.5	40.7	42.9	0	0
C-8Si	300	6.9	0	24.8	2.1	35.5	37.1	0	0
C-9Al	300	18.8	0	11.0	2.4	42.1	44.2	0	0
C-10aAl	300	6.6	0	25.2	1.7	33.8	38.9	0	0

[a] Catalytic results obtained at a reaction temperature = 400 °C and a C_3/O_2/He/steam molar ratio of 4/8/58/30.
[b] Contact time, W/F, in $g_{cat}\,h\,mol_{C_3}^{-1}$.
[c] Space time yield, STY_{AA}, in $g_{AA}\,kg_{cat}^{-1}\,h^{-1}$.
[d] STY'_{AA} is the rate of acrylic acid formation per unit mass of active components (in $g_{AA}\,kg_{MoVTeNb}^{-1}\,h^{-1}$).

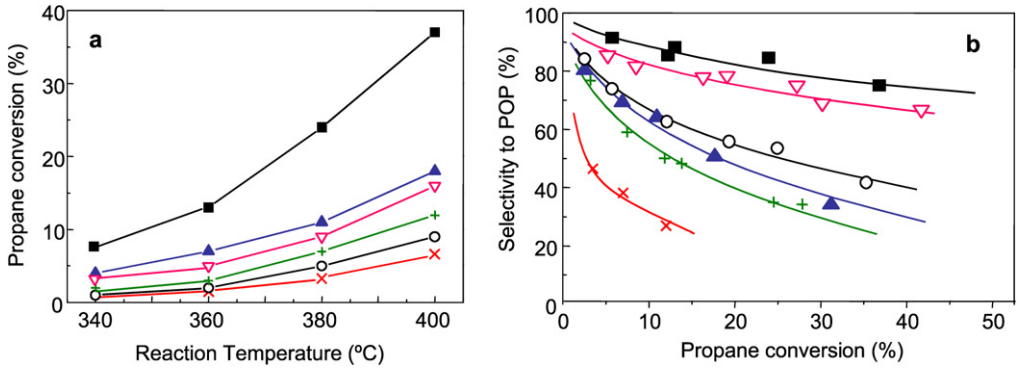

Fig. 5. Variation of the propane conversion with the reaction temperature at a contact time, W/F, of 300g_{cat} h $mol_{C_3}^{-1}$ (a) and variation of the sum of the selectivity to partial oxidation products (POP: propylene, acrylic acid, acrolein, acetone, and acetic acid) with the propane conversion at 380–400 °C (b) on undiluted and diluted Mo–V–Nb–Te catalysts. Symbols: (■) CT-1; (○) CT-2Si; (▲) CT-3Al; (▽) CT-4aAl; (+) CT-5Nb; (×) CT-6Zr.

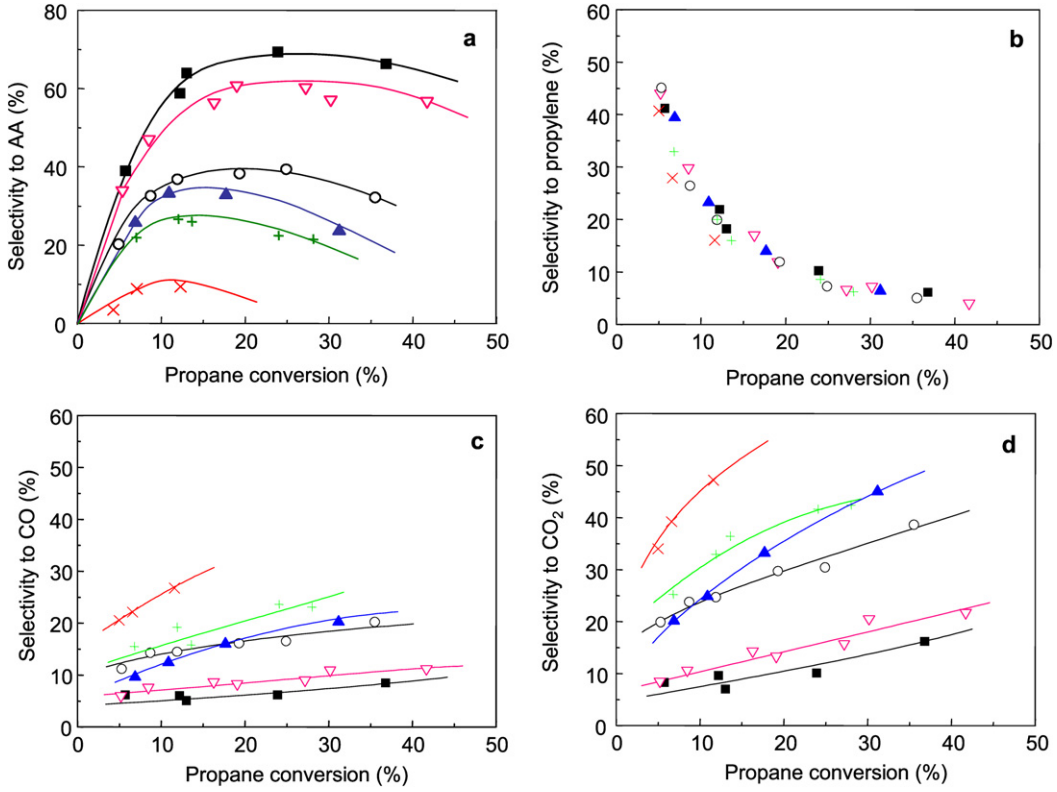

Fig. 6. Variation of the selectivity to acrylic acid (a), propylene (b), CO (c) and CO_2 (d) with the propane conversion, in the 380–400 °C temperature range, during the oxidation of propane over undiluted and diluted Mo–V–Nb–Te catalysts. Symbols: (■) CT-1; (○) CT-2Si; (▲) CT-3Al; (▽) CT-4aAl; (+) CT-5Nb; (×) CT-6Zr.

alytic activity and selectivity to acrylic acid strongly depended on the nature of the diluter incorporated.

No acrylic acid was detected over Te-free catalysts (regardless of the diluter used), although propylene and acetic acid were observed in all cases.

Fig. 5a shows the variation of the propane conversion with the reaction temperature obtained during propane oxidation on Mo–V–Nb–Te catalysts. Accordingly, the catalytic activity for Te-containing catalysts decreased as follows: undiluted > γ-Al_2O_3- > α-Al_2O_3- > Nb_2O_5- > SiO_2- > ZrO_2-containing catalyst.

Fig. 5b plots the variation of the selectivity to partial oxidation products (POP: propylene + acrylic acid + acetic acid) with the propane conversion on Te-containing catalysts. A very high initial selectivity to POP (ca. 90%) was found for all catalysts, but the selectivity to POPs decreased with propane conversion in a different extension, depending on the diluter.

Fig. 6 shows the evolution of the selectivity to the main reaction products (acrylic acid, propylene, CO, and CO_2) with propane conversion at reaction temperatures of 380–400 °C on Mo–V–Nb–Te-containing catalysts. The selectivity to acrylic acid varied as follows: bulk > α-Al_2O_3- ≫ SiO_2- > γ-Al_2O_3- > Nb_2O_5- > ZrO_2-containing catalyst. This indicates that α-Al_2O_3 is preferred as diluter, although this catalyst exhib-

Table 3
Oxidation of propylene on bulk and diluted Mo–V–Nb–Te–O catalysts[a]

Catalyst	W/F[b]	Propylene conversion (%)	Selectivity (%)					STY_{AA}[c]	STY'_{AA}[d]
			Acrylic acid	Acetone	Acetic acid	CO	CO_2		
CT-1	75	86.5	87.2	0.8	0	8.4	3.5	724	724
CT-2Si	150	74.8	78.6	1.0	1.7	8.0	10.4	282	353
CT-3Al	150	78.9	71.9	1.1	1.4	15.5	9.9	272	340
CT-4aAl	150	78.5	83.9	0.8	0.2	10.7	4.3	316	395
CT-5Nb	150	65.3	68.1	1.0	2.6	18.4	9.4	213	266
CT-6Zr	150	54.9	73.7	1.2	1.5	14.9	4.3	194	243

[a] Catalytic results obtained at a reaction temperature = 400 °C, and a $C_{C_3H_6=}/O_2$/He/steam molar ratio of 1.7/6.8/76.5/15.

[b] Contact time, W/F, in $g_{cat}\,h\,mol^{-1}_{C_3=}$.

[c] Space time yield, STY_{AA}, in $g_{AA}\,kg^{-1}_{cat}\,h^{-1}$.

[d] STY'_{AA} is the rate of acrylic acid formation per unit mass of active components (in $g_{AA}\,kg^{-1}_{MoVTeNb}\,h^{-1}$).

ited lower acrylic formation than the corresponding undiluted catalyst.

Also note that among POP, propylene was the main primary reaction product from propane (see Fig. 6b). Meanwhile, similar selectivities to propylene were observed among the bulk and diluted catalysts; the selectivity to CO and CO_2 carbon oxides (Figs. 6c and 6d, respectively) exhibits an opposite trend to that observed for the selectivity to acrylic acid (Fig. 6a). These findings suggest that the most important difference between undiluted and diluted Te-containing catalysts is related to the higher or lower extension of the overoxidation of partial oxidation products.

To investigate the influence of the presence of diluter in the oxidation of reaction intermediates, we also studied the oxidation of propylene over bulk and diluted catalysts. Table 3 summarizes some of the catalytic results obtained for propylene oxidation at 380 °C. As shown, in all of the catalysts studied, the selectivity to acrylic acid remained very high, although the undiluted sample had the highest selectivity to acrylic acid. It also can be seen that the selectivity to acrylic acid during the oxidation of propylene follows the same order as that observed in the oxidation of propane (bulk $> \alpha$-Al_2O_3- $\gg SiO_2$- $> \gamma$-Al_2O_3- $> Nb_2O_5$- $> ZrO_2$-containing catalyst), although the differences are considerably lower in the case of propylene oxidation.

3.2.2. Ethane oxidation

Table 4 summarizes the catalytic results of bulk and diluted MoV(Te)NbO catalysts obtained during the oxidation of ethane at 400 °C. Ethylene, carbon monoxide, and carbon dioxide were observed only as reaction products, with a carbon balance of 100 ± 2% for all catalytic tests. In this case, all of the catalysts exhibited relatively high initial selectivity to ethylene, although Te-containing catalysts were more active and selective in the oxidative dehydrogenation of ethane to ethylene compared with the corresponding Te-free Mo–V–Nb catalysts. In addition, and although all Te-containing catalysts presented similar selectivities to ethylene at low ethane conversions, the catalysts exhibited important differences in catalytic activity for ethane oxidation.

Fig. 7 presents the variation of ethane conversion with the reaction temperature obtained over undiluted and diluted Mo–V–Nb–Te catalysts. It can be concluded that the catalytic activity for ethane conversion decreased in the following order: undiluted $> \alpha$-Al_2O_3- $> \gamma$-Al_2O_3- $> SiO_2$-, Nb_2O_5- $> ZrO_2$-containing catalyst.

Table 4
Oxidation of ethane on diluted Mo–V–Nb–Te–O and Mo–V–Nb–O catalysts[a]

Catalyst	Ethane conversion (%)	Selectivity (%)			$STY_{C_2H_4}$[b]	$STY'_{C_2H_4}$[c]
		Ethylene	CO	CO_2		
CT-1	35.6	93.6	4.0	2.5	245	245
CT-2Si	18.0	95.4	2.8	1.8	126	158
CT-3Al	23.9	93.6	4.0	2.4	165	207
CT-4aAl	29.5	95.0	3.1	1.9	206	258
CT-5Nb	18.8	93.2	4.3	2.5	129	161
CT-6Zr	14.2	93.6	4.4	1.9	97.9	123
C-7	5.5	73.5	19.8	6.8	29.7	37.1
C-8Si	3.5	65.9	24.9	9.2	17.0	21.3
C-9Al	7.8	65.3	25.4	9.3	37.5	46.9
C-10aAl	2.7	63.2	25.7	11.1	12.6	15.8

[a] Catalytic results obtained at a reaction temperature = 400 °C, a C_2/O_2/He molar ratio of 30/10/60; and a contact time, W/F, of 40 $g_{cat}\,h\,mol^{-1}_{C_2}$.

[b] Space time yield, $STY_{C_2H_4}$, in $g_{C_2H_4}\,kg^{-1}_{cat}\,h^{-1}$.

[c] $STY'_{C_2H_4}$ is the rate of ethylene formation per unit mass of active components (in $g_{C_2H_4}\,h^{-1}\,kg^{-1}_{MoVTeNb}$).

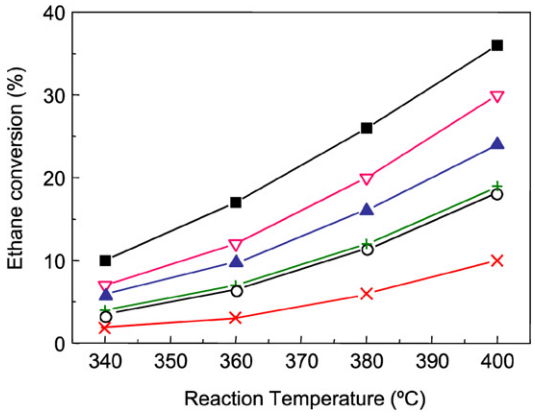

Fig. 7. Variation of the ethane conversion with the reaction temperature at a contact time, W/F, of 40 $g_{cat}\,h\,mol^{-1}_{C_2}$ obtained during the ethane oxidation on undiluted and diluted Mo–V–Nb–Te catalysts. Symbols: (■) CT-1; (○) CT-2Si; (▲) CT-3Al; (▽) CT-4aAl; (+) CT-5Nb; (×) CT-6Zr.

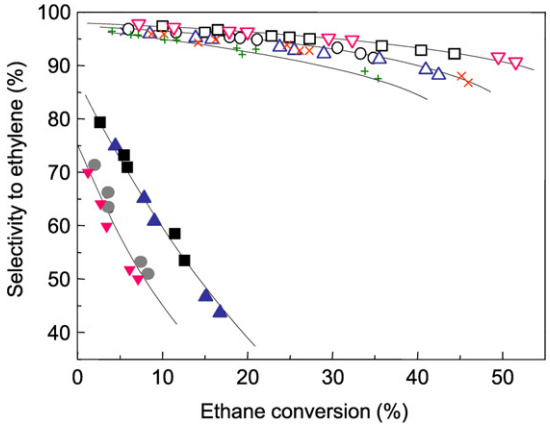

Fig. 8. Variation of the selectivity to ethylene with the ethane conversion in the 380–400 °C temperature range obtained during the ethane oxidation on undiluted and diluted Mo–V–Nb or Mo–V–Nb–Te catalysts. Symbols: (□) CT-1; (○) CT-2Si; (△) CT-3Al; (▽) CT-4aAl; (+) CT-5Nb; (×) CT-6Zr; (■) C-7; (●) C-8Si; (▲) C-9Al; (▼) C-10aAl.

Fig. 8 shows the evolution of the selectivity to ethylene with the ethane conversion in the reaction temperature range of 380–400 °C. Minimal differences in the selectivity to ethylene can be observed at low ethane conversions for Mo–V–Nb–Te catalysts (with selectivities to ethylene of ca. 95% at ethane conversions of 10%), whereas Te-free catalysts demonstrate significantly lower selectivity to ethylene compared with the corresponding Te-containing catalysts.

Small differences in the selectivity to ethylene also can be seen at high ethane conversions over Te-containing catalysts, although both the undiluted and α-Al_2O_3-diluted catalysts present the highest selectivity to ethylene. Moreover, it is evident that overoxidation of ethylene is very important for Te-free catalysts, suggesting that some of the crystalline phases present in these catalysts favor the overoxidation of ethylene.

Based on the results given in Table 4, we can conclude that both the space time yield ($STY_{C_2H_4}$) and the rate of formation of ethylene per unit mass of active components ($STY'_{C_2H_4}$) were higher for the undiluted catalyst than for most of the diluted catalysts. Only in the α-Al_2O_3-containing catalysts was it possible to obtain a catalytic performance similar to that of the undiluted catalyst.

3.3. General remarks

The catalytic results of diluted Mo–V–Nb–Te catalysts during the propane oxidation indicate that they are less active and selective in the formation of acrylic acid than the undiluted catalyst, although this effect depends on the diluent metal oxide incorporated. In this way, the selectivity to acrylic acid for propane oxidation decreased in the following order: bulk > α-Al_2O_3- ≫ SiO_2- > γ-Al_2O_3- > Nb_2O_5- > ZrO_2-containing catalyst.

In agreement with the results presented here, Holmberg et al. [22], studying the ammoxidation of propane and propylene, reported that the dilution of Mo–V–Nb–Te mixed oxides with γ-Al_2O_3, SiO_2, or TiO_2 favored a drastic decrease in both catalytic activity and selectivity to acrylonitrile, as a consequence of the formation of different crystalline phases (which is favoured by the presence of diluter).

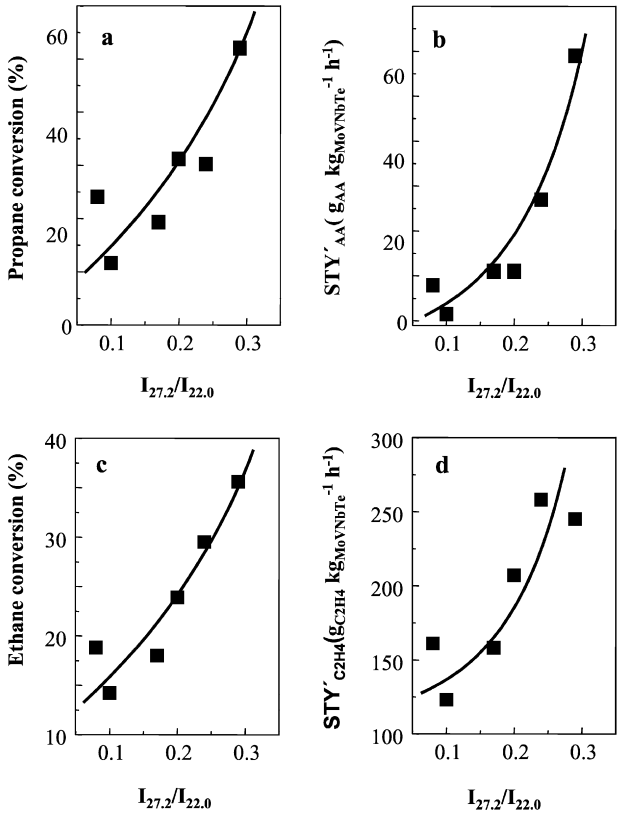

Fig. 9. Variation of the propane conversion (a), the rate of acrylic acid formation per unit mass of active components, STY'_{AA} (b), the ethane conversion (c), and the rate of ethylene formation per unit mass of active components, $STY'_{C_2H_4}$ (d) with the relative presence of the M1 phase ($I_{27.2}/I_{22.0}$ ratio determined by XRD) in undiluted and diluted Mo–V–Nb–Te catalyst. The catalytic results for propane and ethane oxidation from Tables 2 and 4, respectively.

But we observed a different catalytic behavior during ethane oxidation on our diluted catalysts. The catalytic activity decreased following the same trend as for propane oxidation, but little differences in the selectivity to ethylene (at isoconversion conditions) were found among these catalysts (Fig. 8). For this reason, if the changes observed in the nature of crystalline phases in these catalysts were responsible for their catalytic behavior, then the influence of these crystalline phases on the selectivity to acrylic acid for propane oxidation should be different than that on the selectivity to ethylene for ethane oxidation.

According to our characterization results, the formation of crystalline phases other than M1 and M2 depends strongly on the metal oxide diluter. Fig. 9 shows the variation of the conversion of propane (Fig. 9a) and ethane (Fig. 9c) with the $I_{27.2}/I_{22.0}$ ratio obtained from the XRD patterns. For comparison, the figure also compares the variation of the rate of formation of acrylic acid (Fig. 9c) and ethylene (Fig. 9d) per unit mass of active components (i.e., STY'_{AA} and $STY'_{C_2H_4}$ in Tables 2 and 4, respectively) with the $I_{27.2}/I_{22.0}$ ratios obtained for undiluted and diluted catalysts (Table 1). It can be seen that the catalytic activity in the oxidation of both ethane and

propane, as well as the formation of partial oxidation products (i.e., acrylic acid or ethylene), increased with the amount of M1 phase in the diluted Mo–V–Nb–Te catalysts. These findings confirm that M1 phase is the key factor in the selective oxidative activation of ethane and propane [15–23], but they do not completely explain the differences observed in the selectivity to acrylic acid (Fig. 6a) and to ethylene (Fig. 8) over diluted Mo–V–Nb–Te catalyst.

Comparison of the catalytic results over Te-free catalysts demonstrated no acrylic acid from propane in any of these catalysts (Table 2), whereas relatively high selectivity to ethylene was obtained at low ethane conversions during ethane oxidation (Table 4). These results suggest that the presence of crystalline phases other than M1/M2 in diluted catalysts [i.e., M_5O_{14} (M = Mo, V, Nb), $TeMo_5O_{16}$, and supported MoO_x species] has different effects on the overoxidation of the corresponding partial oxidation products.

Mo–V–Nb mixed-metal oxides are active but relatively unselective for the ODH of propane [34–36], although acetic acid also can be observed in M_5O_{14} (M = Mo, V, Nb)-containing catalysts [35]. Moreover, Mo–V–Nb mixed-metal oxides are relatively selective in the ODH of ethane [34,37], but M_5O_{14} (M = Mo, V and/or Nb) demonstrated poor activity in both ethane and ethylene oxidation under the reaction conditions used in the present study (reaction temperature below 425 °C) [38]. Consequently, it has been suggested that the presence of tellurium in Mo–V-containing catalysts not only facilitates the formation of M1 phase, but also inhibits the presence of MoO_2 and some not desirable nonstoichiometric mixed oxides [15,35], which also are unselective in oxidation reactions [37].

On the other hand, supported MoO_x catalysts are active in the ODH of propane to propylene [39,40] but show low selectivity to POPs during the oxidation of propylene [41]. However, supported MoO_x [42] catalysts exhibit very poor activity in both ethane and ethylene oxidation. Finally, $TeMo_5O_{16}$ is active and relatively selective in the propylene oxidation to acrolein [43] but is inactive in ethylene oxidation. Therefore, the presence of M_5O_{14} (M = Mo, V, Nb), or supported MoO_x species in Te-containing catalysts favors the overoxidation of propylene and decreased formation of acrylic acid during the oxidation of propane, and exert only slight influence on the overoxidation of ethylene.

Nevertheless, we must note that the selectivity to acrylic acid from propane on diluted catalysts was lower than that from propylene, and that for the latter, only small differences were observed for the different catalysts. This finding is in agreement with previous observations during propane ammoxidation over diluted Mo–V–Nb–Te catalysts [22] and in the oxidation of propane/propylene over similar mixed-metal oxide catalysts [44–47]. The higher selectivity to acrylic acid from the oxidation of olefin compared with that from the corresponding alkane likely can be related to the differences in the oxidation state of the surface of the catalysts depending on the substrate used, as has been suggested for the oxidation of butenes/*n*-butane [48] or pentenes/*n*-pentane [1] over VPO catalysts. It is known that the catalyst surface is more reduced during the oxidation of olefins than during the oxidation of alkanes, which must be linked to the different selectivities achieved [49]. Thus, a higher oxidation state of the surface (as occurs in propane oxidation) probably favors deep oxidation of POPs, resulting in lower selectivity to acrylic acid than that observed during the oxidation of propylene.

Finally, the varying predominance of M1 phase in bulk and diluted Mo–V–Nb–Te catalysts can be tentatively explained by the partial interaction between the metal oxide diluter and the transition metal cations (especially polymolybdate species) involved in formation of the M1 phase during the evaporation step, changing the effective composition during the synthesis of diluted catalysts. This is in agreement with the formation of $Al_2(MoO_4)_3$ or $ZrMo_2O_8$ observed in γ-Al_2O_3- or ZrO_2-containing catalysts, which supports the interaction between Mo species and some of the metal oxides used as diluters, leading to modifications in both the nature of crystalline phases and the catalytic performance. For this reason, a metal oxide diluter with low surface area and/or low capacity is needed to interact with vanadia and molybdena, as α-Al_2O_3, to maintain the concentration of transition metal cations during synthesis.

SiO_2 and α-Al_2O_3 are known to be less reactive than γ-Al_2O_3, ZrO_2, or Nb_2O_5 with molybdenum species in solution. However, the formation of M2 is also favored in SiO_2- or α-Al_2O_3-diluted catalysts. This suggests that other factors besides the effective concentration of Mo species (e.g., pH of the final solution, partial interaction of M1 and diluter during the calcination step) must play a role in the formation of M1/M2 in diluted catalysts.

4. Conclusion

The incorporation of a metal oxide, such as SiO_2, γ-Al_2O_3, α-Al_2O_3, Nb_2O_5, or ZrO_2, into a MoVTeNbO mixed-metal oxide can improve the physical and mechanical properties of these types of catalysts by modifying both the nature of crystalline phases and the catalytic performance in oxidation reactions. According to our results, a parallelism between the presence of the M1 phase and the catalytic performance for ethane and propane conversion can be proposed, confirming that this is the active phase in the selective oxidative activation of short-chain alkanes.

Nevertheless, a strong influence of the presence of crystalline phases other than M1 and M2 on the selectivity to acrylic acid has been observed during propane oxidation over diluted catalysts. Moreover, the presence of these crystalline phases seems to have only a slight influence on the selectivity to ethylene during the oxidation of ethane over the same catalysts. This could be related to the higher reactivity of POPs observed in propane oxidation (i.e., propylene, acrolein) compared with that of ethylene on the crystalline phases (Mo_5O_{14}, $TeMo_5O_{16}$, or supported MoO_x species) detected in diluted catalysts. In this way, α-Al_2O_3 seems to be the most appropriate diluter for achieving good catalytic performance in the partial oxidation of both ethane and propane.

Acknowledgments

Financial support was provided by the DGICYT of Spain (project CTQ2006-09358/BQU). B.S. thanks the MEC (Ramón y Cajal Programme).

References

[1] F. Cavani, F. Trifiró, Catal. Today 51 (1999) 561.
[2] H.H. Kung, M.C. Kung, Appl. Catal. A 157 (1997) 105.
[3] T. Blasco, J.M. López Nieto, Appl. Catal. A 157 (1997) 117.
[4] M. Bañares, Catal. Today 51 (1999) 319.
[5] H.X. Dai, C.T. Au, Curr. Top. Catal. 3 (2002) 33.
[6] J.M. López Nieto, Top. Catal. 41 (2006) 3.
[7] R.K. Grasselli, J.D. Burrington, D.J. Buttrey, P. DeSanto, C.G. Lugmair, A.F. Volpe, T. Weingand, Top. Catal. 23 (2003) 5.
[8] T. Ushikubo, Catal. Today 78 (2003) 43.
[9] D. Vitry, J.L. Dubois, W. Ueda, J. Mol. Catal. A Chem. 220 (2004) 67.
[10] M.M. Lin, Appl. Catal. A 207 (2001) 1.
[11] T. Ushikubo, H. Nakamura, Y. Koyasu, S. Wajiki, US Patent 5,380,933 (1995); EP 0,608,838 B1 (1997).
[12] T. Ushikubo, K. Oshima, A. Kayo, T. Umezawa, K. Kiyono, I. Sawaki, EP529853 A2 (1993); assigned to Mitsubishi.
[13] T. Ushikubo, K. Oshima, A. Kayou, M. Hatano, Stud. Surf. Sci. Catal. 112 (1997) 473.
[14] J.M. López Nieto, P. Botella, M.I. Vázquez, A. Dejoz, Chem. Commun. (2002) 1906.
[15] P. Botella, E. García-González, A. Dejoz, J.M. López Nieto, M.I. Vázquez, J. González-Calbet, J. Catal. 225 (2004) 428.
[16] J.M.M. Millet, H. Roussel, A. Pigamo, J.L. Dubois, J.C. Jumas, Appl. Catal. A Gen. 232 (2002) 77.
[17] J.M.M. Millet, M. Baca, A. Pigamo, D. Vitry, W. Ueda, J.L. Dubois, Appl. Catal. A Gen. 244 (2003) 359.
[18] P. DeSanto, D.J. Buttrey, R.K. Grasselli, C.G. Lugmair, A.F. Volpe, B.H. Toby, T. Vogt, Z. Kristallogr. 219 (2004) 152.
[19] H. Tsuji, K. Oshima, Y. Koyasu, Chem. Mater. 15 (2003) 2112.
[20] P. Botella, E. García-González, J.M. López Nieto, J.M. González-Calbet, Solid State Sci. 7 (2005) 507.
[21] H. Murayama, D. Vitry, W. Ueda, G. Fuchs, M. Anne, J.L. Dubois, Appl. Catal. A 318 (2007) 137.
[22] J. Holmberg, R. Häggblad, A. Andersson, J. Catal. 243 (2006) 350.
[23] J.M. Oliver, J.M. López Nieto, P. Botella, A. Mifsud, Appl. Catal. A Gen. 257 (2004) 67.
[24] A. Corma, V. Fornés, M.I. Juan-Rajadell, J.M. López Nieto, Appl. Catal. A 116 (1994) 151.
[25] I.E. Wachs, J.-M. Jehng, W. Ueda, J. Phys. Chem. B 109 (2005) 2275.
[26] H. Knözinger, H. Jezlorowski, J. Phys. Chem. 82 (1978) 2002.
[27] H. Hu, I.E. Wachs, S.R. Bare, J. Phys. Chem. 99 (1995) 10897.
[28] G. Mestl, T.K.K. Srinavasan, Catal. Rev.-Sci. Eng. 40 (1998) 451.
[29] Y.S. Jin, A. Auroux, J.C. Vedrine, J. Chem. Soc. Faraday Trans. 1 85 (1989) 4179.
[30] Z. Liu, Y. Chen, J. Catal. 177 (1998) 314.
[31] M. Roussel, M. Bouchard, E. Bordes-Richard, K. Karim, S. Al-Sayari, Catal. Today 99 (2005) 77.
[32] G. Mestl, J. Raman Spectrosc. 33 (2002) 333.
[33] M. Dieterle, G. Mestl, Phys. Chem. Chem. Phys. 4 (2002) 822.
[34] A. Adesina, N.W. Cant, A. Saberi-Moghaddam, C.H.L. Szeto, D.L. Trim, J. Chem. Technol. Biotechnol. 72 (1998) 19.
[35] P. Concepción, P. Botella, J.M. López Nieto, Appl. Catal. A 278 (2004) 45.
[36] Z. Zhao, X. Gao, I.E. Wachs, J. Phys. Chem. B 107 (2003) 6333.
[37] M. Mezourki, B. Taouk, L. Tessier, E. Bordes, P. Courtine, Stud. Surf. Sci. Catal. 75 (1993) 753.
[38] J.M. López Nieto, P. Botella, P. Concepción, A. Dejoz, M.I. Vázquez, Catal. Today 91–92 (2004) 247.
[39] K. Chen, S. Xie, A.T. Bell, E. Iglesia, J. Catal. 198 (2001) 232, and references therein.
[40] E. Heracleous, M. Machli, A.A. Lemonidou, I.A. Vasalos, J. Mol. Catal. A 232 (2005) 29.
[41] C. Martin, I. Martin, C. Mendizábal, V. Rives, Stud. Surf. Sci. Catal. 75 (1993) 1987.
[42] A. Chistodoulakis, E. Heracleous, A.A. Lemonidou, S. Boghosian, J. Catal. 242 (2006) 16.
[43] P. Botella, J.M. López Nieto, B. Solsona, J. Mol. Catal. A 184 (2002) 335.
[44] M. Lin, T.B. Desai, F.W. Kaiser, P.D. Klugherz, Catal. Today 61 (2000) 223.
[45] P. Botella, J.M. López Nieto, B. Solsona, A. Mifsud, F. Márquez, J. Catal. 209 (2002) 445.
[46] E.K. Novakova, J.C. Vedrine, E.G. Derouane, J. Catal. 211 (2002) 235.
[47] W. Ueda, D. Vitry, T. Katou, Catal. Today 96 (2004) 235.
[48] G. Centi, F. Trifiró, J.R. Ebner, V.M. Franchetti, Chem. Rev. 88 (1988) 55, and references therein.
[49] G. Centi, G. Fornasari, F. Trifió, J. Catal. 89 (1984) 44.